VALIDATION OF AEROACOUSTIC PREDICTIONS USING THE HELINOVI DATABASE

M. Pidd[1], A. Dummel[2], D. Falchero[3], M. Genito[4],
J Prospathopoulos[5], A. Visingardi[4], S.G. Voutsinas[5], J. Yin[6]

[1] QinetiQ, United Kingdom
e-mail: mpidd@QinetiQ.com

[2] EUROCOPTER (ECD), Germany
e-mail: andreas.dummel@eurocopter.com

[3] EUROCOPTER (ECF), France
e-mail: daniele.falchero@eurocopter.com

[4] Centro Italiano Ricerche Aerospaziali, (CIRA), Italy
e-mail: m.genito@cira.it, a.visingardi@cira.it

[5] National Technical University of Athens (NTUA) Greece
e-mail: jprosp@fluid.mech.ntua.gr, spyros@fluid.mech.ntua.gr

[6] Deutsches Zentrum für Luft- und Raumfahrt (DLR), Germany
e-mail: jianping.yin@dlr.de

Key words: Complete rotorcraft, Aeroacoustics, Tail rotor noise validation, HeliNOVI

Abstract: The European research project HeliNOVI was aimed at the enhancement of helicopter performance, safety and ride comfort. Within this project one of the principal aims was the study of the aerodynamics and aeroacoustics of the tail rotor in order to reach a deeper knowledge of the phenomena related to it. A key activity was the design of a wind tunnel test employing the existing powered 40%-scaled BO105 helicopter model for the generation of a high-quality database for code validation and assessment of tail rotor noise reduction means and the exploitation of this database for the validation of simulation codes. This validation activity included code-to-code and code-to-test comparisons using the predicted and wind tunnel results.

A validation activity for acoustic prediction results from six of the HeliNOVI partners has been performed. The details of the range of partners' methods applied for aircraft trim, wake modelling, aerodynamic and aeroacoustic solutions are described. The numerical/experimental comparisons of the results obtained by the partners show a significant variation in the level of agreement with the HeliNOVI experimental data, but generally capture some of the interaction effects between main and tail rotors. Loading noise often dominates the results and it is found that the trim methodology is crucial to the acoustic prediction. Indeed the large variation in the acoustic predictions is largely due to the variation in the results of the preceding aerodynamic analyses. The HeliNOVI database of experimental and predicted dynamic, aerodynamic and aeroacoustic data provides a valuable asset for further development and validation of acoustic prediction capabilities.

1 INTRODUCTION

Background

The conventional helicopter is close to the edge of its performance envelope; for the future, emphasis will be laid on making it a more efficient and environmentally friendly means of transport. The European helicopter manufacturers are already producing the quietest helicopters in the world; furthermore, they are the market leaders in civil helicopters. In order to maintain this position an ongoing continuous research activity to support the industry is mandatory. This has been the primary objective of a series of research projects of which the HeliNOVI project (Helicopter Noise and Vibration) European research can be considered a logical continuation.

HeliNOVI [1] was aimed at the enhancement of helicopter performance, safety and ride comfort. Within this programme approximately half the effort was devoted to the aerodynamic and aeroacoustic studies of the tail rotor in order to reach a deeper knowledge of the phenomena related to it. The key activities of this work concerned:

- the adaptation, upgrade or refinement of rotor aerodynamic and acoustic simulation codes for the prediction of high resolution unsteady blade surface pressures and the radiated noise;
- the design of a wind tunnel test employing the existing powered 40%-scaled BO105 helicopter model for the generation of a high-quality database for code validation and assessment of means for reduction of the tail rotor noise;
- the validation of the simulation codes;
- the numerical and experimental quantification of the tail rotor noise reduction potential through variation of blade air load and tip speed, change of the tail rotor sense of rotation and the modification of the tail rotor position, with the aim of assessing the acoustic benefits in view of realistic helicopter operation and eventually of establishing design guidelines for future quieter helicopters with conventional tail rotors.

The work reported in this paper was a part of a larger validation activity aimed at the validation of the aeroacoustic prediction codes through the performance of code-to-code and code-to-test comparisons using the predicted and wind tunnel results. It represents the concluding step of the improvement process in the computational tools, already initiated through the preliminary activity of adaptation of the available computer codes, in order to meet the requirements for high resolution when simulating the main rotor (MR) / tail rotor (TR) interactive behaviour. As a first step for this activity a number of pre-test predictions were performed and the results were presented at the 31st European Rotorcraft Forum [2].

Two research centres: CIRA (I) and DLR (D), a university: NTUA (GR), industry partner QinetiQ (UK), and manufacturing industry partner EUROCOPTER (D, Fr) participated in these activities. In particular, the experimental dataset was post-processed and provided by DLR to the partners. The detailed information on this activity is detailed in references [3], [4] and [5].

Outline of the paper

The present paper together with partnering papers [6] and [7] aim to illustrate the final numerical aerodynamic and aeroacoustic validation activity performed by the HeliNOVI

partners through code-to-code and code-to-test comparisons with the experimental data produced during the project's wind tunnel test campaign and the exploitation of the results for the evaluation of means of helicopter noise reduction. Reference [6] provides a validation of the aerodynamics results on which the current acoustic results are crucially dependent. Reference [7] details the exploitation of both experimental and numerical results for the evaluation of the various means of tail rotor noise reduction studied within the HeliNoVi project.

A short description, aimed at illustrating the main geometrical and instrumentation characteristics of the BO105 model, is given in Section 2. Section 3 provides a description of the test cases performed by the partners for the final validation of the aerodynamic prediction tools. The methodologies applied as well as the trim procedures followed are briefly described in Section 4. An introduction to the presentation of the results and details of some issues in their interpretation are given in Section 5. An analysis of the results is provided in detail in Section 6. The conclusions close the paper in section 7.

Throughout the paper a common numbering of HeliNOVI partners is used which is consistent with that used in references [6] and [7].

2 THE WIND TUNNEL TEST

The wind tunnel model, shown in Figure 1, consists of main rotor (MR) blades and a geometrically scaled fuselage including teetering tail rotor (TR) system [8]. The backbone of the model is the MWM (Modular Wind tunnel Model, [9]) containing, in a shell core, components like gearbox, rotor shaft and drive train system for the MR.

For the HeliNOVI wind tunnel test campaign the BO105 model was tested in the German-Dutch Wind Tunnels (DNW) Large-Low speed Facility (LLF) consisting of an 8m x 6m open jet test section.

The model

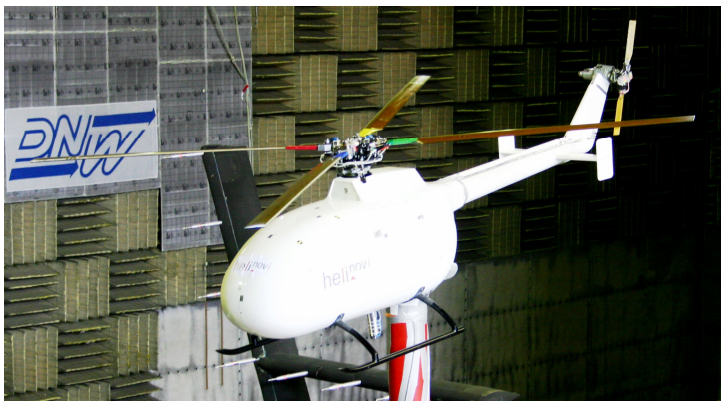

Figure 1: The BO105 wind tunnel model

The MR is a geometrically and dynamically scaled model of the four-bladed hingeless BO105 MR with a NACA23012 aerofoil whose trailing edge was modified to form a 5 mm long tab in order to match the geometry of the full scale rotor. The blades have a linear twist of -8° and a rectangular planform leading to a solidity of 0.077. The TR is a geometrically scaled model of the two-bladed BO105 see-saw TR. The blades have no twist and a standard square tip.

Two sets of TR blades were used; one with S102 aerofoil sections and one with NACA0012 aerofoil sections. The fuselage is only geometrically similar to the BO105 rotorcraft since the design and manufacture of a dynamically scaled helicopter fuselage is beyond the available technology for helicopter wind tunnel models.

The MR and TR main characteristics of the model are given in Table 1 below.

Property	symbol	main rotor	tail rotor
no. of blades	N_b	4	2
rotor type		hingeless	teetering
radius	R	2m	0.383m
radius scale factor	S	2.456	2.48
chord	c	0.121m	0.074m
root cutout	r_a	0.44m	0.16m
solidity	σ	0.077	0.123
precone	β_p	2.5^o	0^o
pretwist	Θ_t	$-8^o/R$	$0^o/R$
pitch-flap coupling	Δ_3	0^o	45^o
reference tip Mach	M_{tip}	0.64	0.65
lock number	γ	8	4.2
shaft tilt forward	$\epsilon_t,\ \epsilon_x$	3^o	4.2^o
shaft tilt upward	ϵ_z	90^o	3^o
motor axis upward	ϵ	0^o	50^o
airfoil		NACA23012mod	S102E, NACA 0012
drag area	A_{TR}	-	$0.026m^2$
drag coefficient	$C_{w,TR}$	-	0.8

Table 1: MR and TR characteristics

Note that for this acoustic test the tail rotor was run at a slightly slower speed (approx. 6% slower) than appropriate for the scaled BO105. The objective of this was to provide an integer ratio between main and tail rotor speeds in order to facilitate numerical simulation, in this case 5 tail rotor revolutions to each main rotor revolution. This resulted in a tail rotor tip Mach number of 0.61. It is not believed that this change had any significant impact on the character of the interaction between main and tail rotors.

Instrumentation

The microphone traverse is made up of 16 microphones forming a U shape which is traversed below the model as show in figure 2.

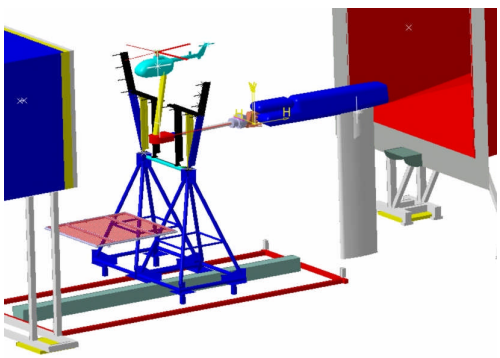

Figure 2: Microphone traverse (in black) below the BO105 wind tunnel model

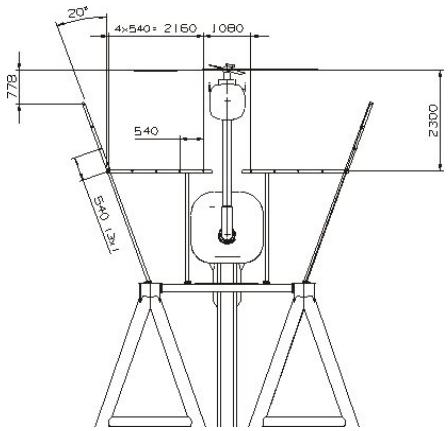

Figure 3: Detail of the microphone traverse

Figure 3 gives details of the microphone traverse set-up in the wind tunnel. The detailed cross flow positions of the microphones are given in Table 2 and Table 3. Level flight and descent condition positions are given in Table 2. For the 12 degree climb case the model had to be lowered and so the locations of the microphones were modified as in Table 3. In most of the cases the microphone rake traversed from 4m ahead of the main rotor to 4m downstream of the main rotor, a two rotor diameter range, at 0.5m intervals.

Mic #	Ymic (m)	Zmic (m)	Mic #	Ymic (m)	Zmic (m)
1	-3.254	-0.778	9	0.540	-2.300
2	-3.069	-1.285	10	1.080	-2.300
3	-2.885	-1.793	11	1.620	-2.300
4	-2.700	-2.300	12	2.160	-2.300
5	-2.160	-2.300	13	2.700	-2.300
6	-1.620	-2.300	14	2.885	-1.793
7	-1.080	-2.300	15	3.069	-1.285
8	-0.540	-2.300	16	3.254	-0.778

Table 2: Microphone co-ordinates

Mic #	Ymic (m)	Zmic (m)	Mic #	Ymic (m)	Zmic (m)
1	-3.254	-0.478	9	0.540	-2.000
2	-3.069	-0.985	10	1.080	-2.000
3	-2.885	-1.493	11	1.620	-2.000
4	-2.700	-2.000	12	2.160	-2.000
5	-2.160	-2.000	13	2.700	-2.000
6	-1.620	-2.000	14	2.885	-1.493
7	-1.080	-2.000	15	3.069	-0.985
8	-0.540	-2.000	16	3.254	-0.478

Table 3: Microphone co-ordinates for climb

3 TEST CASES

Acoustic test cases

Within the HeliNOVI project, validation of the acoustics has been performed against a wide selection of test cases [10]. In the present paper validation of the aeroacoustic prediction codes is performed by making the numerical/experimental comparisons on the four test cases in Table 4, selected from the large dataset available from the HeliNOVI test. This set is chosen to represent the baseline conditions for the noise reduction potentials and to give a broad representation of partner results. Table 5 gives the flight conditions for these cases. Additional validation is presented in references [10] and [11].

ID1	12º climb at 33m/s equipped with a S102 tail rotor blade aerofoil section
ID2	level flight at 60m/s equipped with a S102 tail rotor blade aerofoil section
ID5	6º descent flight at 33m/s equipped with a S102 tail rotor blade aerofoil section
ID13.2	level flight at 60m/s equipped with a NACA0012 tail rotor blade aerofoil

Table 4: Acoustic validation test cases

	Simulated Flight Cond. in W. T.					Main Rotor				Tail Rotor		
ID #	mass (kg)	θ_{FP} (deg)	V∞ (m/s)	M∞	α_{Sh} (deg)	$M_{\Omega R}$	μ	$10^4 \cdot C_T$	α_{TPP} (deg)	$M_{\Omega R}$	μ	$10^4 \cdot C_T$
1	2300	12	33	0.097	-13.1	0.641	0.151	52.9	-13.9	0.614	0.141	90.9
2	2300	0	60	0.176	-6.8	0.641	0.275	52.0	-6.4	0.614	0.256	54.5
5	2300	-6	33	0.097	4.2	0.641	0.151	50.4	+4.0	0.614	0.141	27.5
13.2	2300	0	60	0.176	-6.8	0.641	0.275	52.0	-6.4	0.614	0.256	54.5

Table 5: Acoustic test cases

Each of the above mentioned test cases was selected in order to check the capabilities of the prediction codes to evaluate the aerodynamic and aeroacoustic characteristics of the configuration in different flight conditions. The baseline conditions chosen are:

- ID1, a 12º climb at 33m/s
- ID2, a level flight at 60m/s
- ID5, a 6º descent at 33m/s.

In addition ID13.2, a level flight at 60m/s using a NACA0012 tail rotor blade, is included to provide a full representation of partner results.

ID1 was selected in order to check the codes, particularly with respect to the main rotor as little or no interaction is expected between the main and tail rotor in this case. ID2 and ID13.2 are moderate/high speed test cases where some compressibility effects can be expected at the tip region. They only differ in the aerofoil section of the tail rotor, with ID2 using the BO105's S102 tail rotor whilst ID13.2 uses a NACA0012 tail rotor section suitable for the experimental implementation of the reversed direction of TR rotation. ID5 is a descent flight where main rotor BVI is expected to play an important role. The additional test cases, considered within the HeliNoVi project in order to study potential means of noise reduction, are reported elsewhere [7].

Each partner produced results for a subset of these test cases. Table 6 summarises the distribution of these test cases among the partners:

Test Case	Partner 1	Partner 2	Partner 3	Partner 4	Partner 5	Partner 6
ID1; Climb		X	X	X		
ID2; Level flight		X	X	X	X	X
ID5; Descent	X			X		X
ID13.2; Level flight	X				X	X

Table 6: Test Case distribution among the partners

4 METHODOLOGY AND TRIM PROCESS

Aerodynamic methodology

Partner 1 applied a chain of codes which benefited from its experience with comprehensive codes and included aeroelastic effects. In particular, with reference to BVI, a special 2D model was developed which deals, in a fine space and time scale, with the interaction of vortex structures with the blades. Compressibility was taken into account by using the Prandtl-Glauert compressibility correction formula. The fuselage was not modelled.

Partner 2 applied a commercial comprehensive rotorcraft code which is based on blade element theory. All calculations were performed with elastic blades and in incompressible mode. A plug-in of another comprehensive code further enhanced the aerodynamic ability by offering a constant vorticity contour free wake model as well as a panel method that allowed the aerodynamic modelling of the fuselage for all test cases.

Partner 3 applied an incompressible, unsteady, panel code which is based on the direct potential representation to model the whole BO105 configuration under the hypothesis of rigid body motion. All the computations were performed in incompressible mode.

Partner 4 applied a free-wake incompressible, unsteady panel code which differs from Partner 3's code by using a velocity-based, indirect potential formulation, with a combination of source and dipole distribution used on the solid surfaces and dipole panels in the wake. All the computations were performed in incompressible mode, the fuselage was not modelled and the rotor blades were considered as rigid.

Partner 5 applied a chain of codes to the problem. Initially a wind-tunnel trim procedure was applied, using a free-wake model for the non-interacting main and tail rotors. A subsequent time-domain calculation was performed, using the pre-calculated control cyclics and collectives, for the interacting main and tail rotor configuration. Both these calculations include elastic effects using tools from the partner's comprehensive code suite. A final aerodynamic analysis was performed using a full-potential code incorporating aeroelastic and wake interaction effects, from both rotors, through imposed transpiration velocity conditions. The fuselage was not modelled.

Partner 6 applied an integrated model capable of performing aerodynamic and aeroelastic calculations simultaneously. The aerodynamic part is based on an unsteady vortex particle model coupled with a low-order panel method. The computations were corrected for compressibility effects by using the Prandtl-Glauert formula. The fuselage was not taken into account.

Table 7 summarises the configuration modelling parameters applied by the partners for the final validation computations.

	Compressibility	Blade Flexibility	Fuselage Modelling
Partner 1	Prandtl-Glauert	YES for MR blade	NO
Partner 2	NO	YES	YES
Partner 3	NO	NO	YES
Partner 4	NO	NO	NO
Partner 5	Full Potential	YES	NO
Partner 6	Prandtl-Glauert	YES	YES

Table 7: Configuration modelling parameters & Trim procedures

Trim methodology

Table 8 gives the experimental forces and moments for test cases analysed by the partners. They constitute the reference values for the trim calculations performed by the partners.

TestPoint	Fx_CG [N]	Fy_CG [N]	Fz_CG [N]	Mx_CG [Nm]	My_CG [Nm]	Fz_CG [N]	ThrustTR [N]
ID1	-112.9	151.8	-3818.4	-63.3	268.8	-3818.4	160.0
ID2	-631.6	58.4	-3695.2	-5.9	431.6	-3695.2	102.9
ID5	-115.9	-3.7	-3750.1	-8.5	190.6	-3750.1	39.1
ID13.2	-741.8	120.0	2.6	64.0	66.1	2.6	93.4

Table 8: WT experimental forces and moments

The procedures applied by each partner are briefly described as the follows:

Partner 1 performed both a force and a control angle trim procedure for the main rotor calculations through the application of an aeromechanics code. For the tail rotor, a force trim procedure was used in each case;

Partner 2 evaluated the trim control angles through the application of a force trim procedure to match the experimental MR thrust and moments and the TR thrust;

Partner 3 used the measured trim control angles, apart from the collective pitch values which were modified in order to obtain an average value of both MR and TR thrust coefficients equal to the experimental values;

Partner 4 evaluated the trim control angles through the application of a force trim procedure to match the experimental MR thrust, pitching and rolling moments. The trim procedure was started with the isolated MR. After MR thrust, pitching and rolling moments were reached, matching with the experimental value, the TR was then added into the computation and the TR trim started by assuming that the effect of TR would not change the MR trim value;

Partner 5 derived an initial trim to the MR thrust and moments. The TR was trimmed to thrust alone. The collectives and cyclic resulting from this initial non-interacting calculation were then applied to the full simulation;

Partner 6 evaluated the trim control angles by the application of a force trim procedure to match the experimental MR thrust and moments and the TR thrust.

Table 9 summarises the configuration modelling parameters and the trim procedures applied by the partners for the final validation computations.

	Trim Procedure
Partner 1	Force Trim & Control Angle Trim
Partner 2	Force Trim
Partner 3	Experimental cyclic with collective pitch modification to match the experimental CTs
Partner 4	Force Trim
Partner 5	Force Trim
Partner 6	Force Trim

Table 9: Configuration modelling parameters & Trim procedures

Acoustic methodology

The aeroacoustic methodology of each partner is indicated below.

Partner 1 used a numerical acoustic network to compute the main and classical tail rotor rotational noise levels from the blade pressure distribution, and the Ffowcs-Williams and Hawkings analogy formulation in the time domain. It calculates and propagates the thickness and loading noise at the observer position, except for quadrupole noise. A post processor adds Doppler effects, atmospheric absorption and ground reflections for predicting the rotor noise in real helicopter flights and then expresses the noise level in certification units with trajectory duration effects. The required input data are the observer location, the blade geometry, the trim conditions and the corresponding airloads (i.e. chordwise pressure distribution at each aerofoil along the span) which are provided by aerodynamic codes. The output includes the acoustic pressure signature in the time domain, the spectral analysis (frequency domain) and the noise contour plots over a prescribed region.

Partner 2 used the same method as the acoustical model used by Partner 4 (see later).

Partner 3 used an "all purpose" library of algorithms based on integral methods developed in-house. The main features are:

- designed to be easily coupled with any CFD code, both structured or unstructured;
- based on a "forward" approach in time: requires only the data (e.g. velocity and pressure) relative to the current time step and so any unsteady field can be studied, with no limitations;
- can handle an arbitrary number of systems of reference in arbitrary motion.

In the HeliNOVI project the library has been used in its "Linear-FWH functionality" in order to be coupled with the RAMSYS aerodynamic code. This uses the well-known Farassat 1A formulation [12].

Partner 4 used an aeroacoustic formulation based on the acoustic analogy, Formulation 1 or 1A of Farassat [12], in which the unsteady pressure distribution on the blade surface is required. A new formulation based on unsteady blade air loads as an input for aeroacoustic computation has been derived and implemented. The information required for the thickness noise is purely based on the kinematics and geometry of the blade. The thickness noise is highly directional and the contribution of thickness noise on total noise is predominantly in–plane with the rotor, while the loading noise effects are strongest out of the rotor plane.

Partner 5 used codes which are based on the acoustic analogy approach. The thickness noise is based purely on geometric considerations while the force noise, due to blade loading, takes loading data from either the comprehensive or full-potential code. A summation of the thickness and force contributions gives the total noise.

Partner 6 used the aeroacoustic formulation of Succi. The blade is discretized into elementary sections, each one possessing finite volume. During the motion of the blade, each section displaces fluid of equal volume. The fluid exerts a force normal to the surface element and receives its reaction. By this procedure, each elementary section constitutes a noise source. The summation of the contributions of the discrete noise sources gives the total acoustic pressure. The formulation of Succi is equivalent to the formulation 1A of Farassat [12]. In

order to confirm this equivalence, a second acoustic model based on the Farassat 1A formulation was developed and used for the same cases. The results were found to be in exact agreement with those of the Succi's formulation.

It may be summarised that all of the acoustic formulations are expected to provide good estimates of the force and thickness noise contributions, and that the variation in the solutions is likely to be due to the different aerodynamic results used as inputs.

5 NOTES ON EXPERIMENTAL RESULTS

Three presentations of data are given in this paper:

- time histories of the acoustic pressure at microphone positions;
- frequency spectra at microphone positions;
- contours of Overall Sound Pressure Level (OASPL) and full scale A-weighted OASPL along the microphone array track.

Results are available for time and frequency domains at all 16 microphone positions and at 4 traverse positions (-4.0m, -2.0m, 0.0m and 2.0m). The co-ordinate system is such that the X distance is measured positive downstream with the origin at the main rotor position, thus a microphone at a position of -4.0m is upstream of the main rotor. The microphones are numbered as in tables 2 and 3 with microphone 1 on the MR advancing side and microphone 16 on the MR retreating side. Three microphones at each end of the traverse are above the base of the traverse. Although these results are all reported in reference [10] this paper concentrates on two positions; ahead of and below the main rotor on the advancing side where the main rotor is likely to dominate and below the main rotor slightly to the starboard side where the tail rotor influence is strong.

Carpet plots, such as Figure 6, are presented for Sound Pressure Level with a full scale A-weighting. Full-scale dB(A) values were obtained by first converting the dB value to full-scale (frequencies divided by 2.5) and then applying the A-weighting. These results are not available for all cases but are included where such comparison is considered useful.

The discussion focuses on the time domain and spectral results as these are more useful for detailed validation of the aeroacoustic predictions. Common colour legends are used throughout with all the figures using a common partner legend.

Before a detailed discussion of the experimental results some preliminary comments on the experimental data are required. Significant effort has been expended within the HeliNOVI project on processing the raw wind tunnel data to produce validation data and useful lessons have been learnt.

Phase

The processing of the experimental data requires the use of a trigger signal which is derived from either the main or the tail rotor phase. The origin of the signal used for generating averaged data has a significant impact on the processed data. The two plots in Figure 4 show the acoustic pressure history based upon a main rotor average (green) and an average over 5 revolutions of the tail rotor (5TR) (red) where trigger signals for the different rotors are used for data reduction. These data are shown for two streamwise positions for the same

microphone. It can be seen that the two streamwise positions show different phase relationships between the two microphone positions with different methods of averaging.

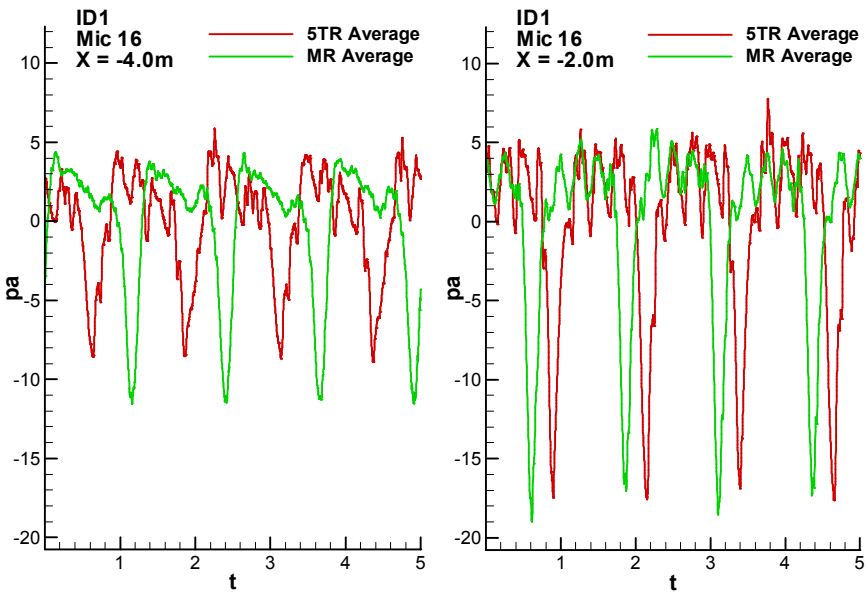

Figure 4: MR/5TR phase

This lack of phase agreement is a result of phase difference within the different experimental data because the two rotors are not synchronised but driven independently so that the trigger signal for the data acquisition started at different times depending on whether it was triggered with respect to 1/MRev or 1/TRev. Although an averaging method was developed in [5] in which the correlation of the MR/TR phase was used to remedy the phase difference in averaging of the TR blade pressures, this method has yet to be applied to the acoustic data. The phase creep means that a uniform correction cannot be applied to match the two time histories. Indeed the time taken to move the microphone rake allows a different phase relationship to develop for different streamwise positions of the rake. The impact of this is an unknown phase difference between the streamwise locations of the microphone rake and an equally unknown phase relationship between these acoustic data and the aerodynamic data processed separately.

The handling of the phase creep within the data is discussed in the following section.

Averaging

Two averaging techniques are applied to reduce the experimental data; one based on the main rotor position (MR) and one on the tail rotor position (5TR), remembering that there is a 5:1 ratio between tail rotor and main rotor rotational speeds. Occasionally, due to experimental problems, averages may not be available from one of the averaging techniques. Where data is based on the tail rotor signal an average over 5 tail rotor rotations is used. In addition, monitoring of the actual phase difference between main and tail rotors ensures that only data with a similar MR/TR phase relationship is included in any set of averaged data.

A comparison of the two averaging techniques is shown, for ID1 60m/s level flight, in Figure 5 for a position ahead of the main rotor on the advancing side. Looking first at the time history (left) it should be noticed that the two averaged results show similar characteristics, hence a good matching of main and tail rotor speeds was achieved. Both averages have

captured main rotor influences (4/rev) with similar magnitude; hence the creep of the TR is seen to be small. The phase shift in the main rotor peaks is due to the starting location of the 5TR averaging when a main rotor blade is not at zero azimuth. The main rotor average, shown in blue, does not capture well all the tail rotor (20/rev) peaks although some TR influence is seen.

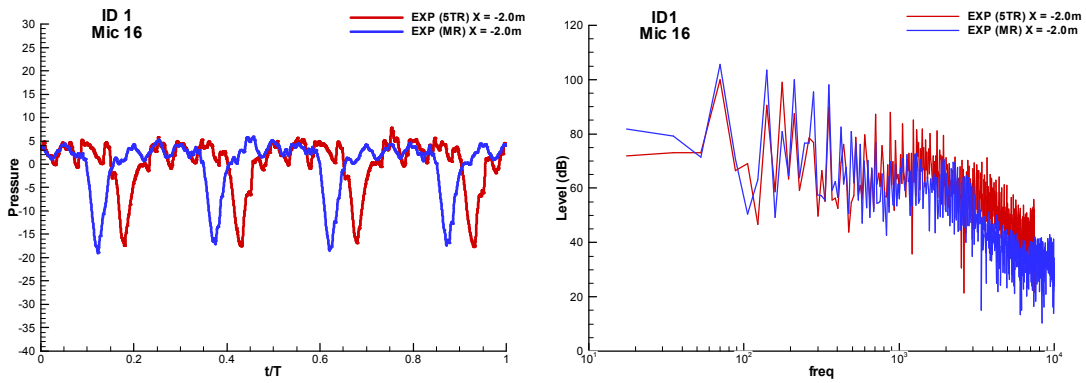

Figure 5: ID1 Experimental pressure history and spectrum

In the frequency domain a slight under prediction of the first few main rotor tones is seen. At higher frequencies the 5TR average shows higher levels than the MR average as the higher tail rotor tones are dominating. This needs to be recognised when looking at averaged results so that appropriate comparison may be made. The impact of A-weighting on these averages is discussed below.

Weighting

When examining contour plots the whole frequency spectrum is reduced to a single value, the Overall Sound Pressure Level (OASPL) at each microphone position. This pressure level is a summation across the frequency spectrum. Where useful, an A-weighted frequency is used to account for the response of the human ear. In all these results a scaled frequency is used, this is the frequency representative of the full scale BO105.

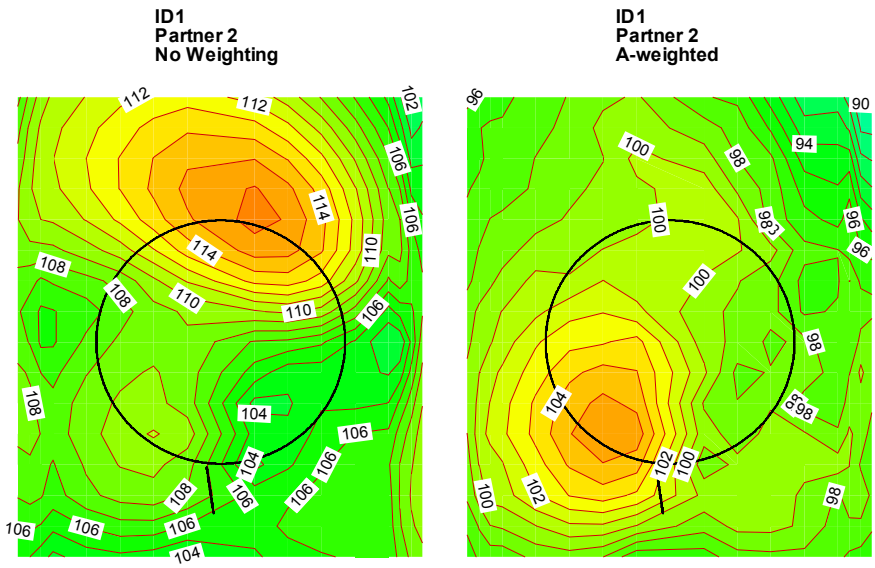

Figure 6: Effect of A-weighting on contour plots.

Figure 6 shows the effect of the application of a full-scale A-weighting to the spectrum. In this figure the flight direction is up the page with the outline of main and tail rotors shown in black. The left (un-weighted) side of the figure shows high levels below the front of the main rotor with lower levels below the thrust side of the tail rotor. In contrast the right (A-weighted) figure shows higher levels in the region of the tail rotor with a lesser effect due to the main rotor. Hence the full-scale A-weighting places a stronger emphasis on the influence of the tail rotor due to its higher frequency content. This is considered appropriate as the A-weighting reflects the frequency response of the human ear and ultimately it is the disturbance produced by the aircraft that governs its potential use.

6 RESULTS FOR VALIDATION CASES

Case ID1; Climb

This test case was analysed by three partners: Partner 2, Partner 3 and Partner 4. The following main control angles and force coefficients were obtained by the application of the computational tools for the trim condition evaluation and aerodynamic analysis:

	CT_{MR}	CQ_{MR}	CT_{TR}	CQ_{TR}
EXP	0.00538	0.000419	0.00652	0.000617
Partner 2	0.00539	0.000488	0.00613	0.000319
Partner 3	0.00542	-	0.00667	-
Partner 4	0.00521	-	0.00649	-

Table 10: ID1 – Main forces and control parameters

Null entries in the table indicate that these data were unavailable from the numerical simulation. In each case the simulations produce a main rotor collective close to that of the experiment with a small under prediction in tail rotor collective. Both main and tail rotor thrusts are well captured. The cyclics were found to be less consistently captured, particularly the longitudinal cyclic.

All the experimental results for this case are based on the 5TR averaged experimental data so main rotor effects may not be clearly seen due to lack of synchronisation between the rotors.

The time histories, plotted in Figure 7, show general agreement in the magnitude of the acoustic pressure with both main rotor (4/rev) and tail rotor (10/rev) behaviour present in both experiment and prediction. For this microphone just ahead of the rotor, close to the centre line, the figure shows a capture of the 4/rev main rotor behaviour. All the results show clear evidence of the 10/rev influence of the tail rotor at similar levels lower than the main rotor 4/rev levels.

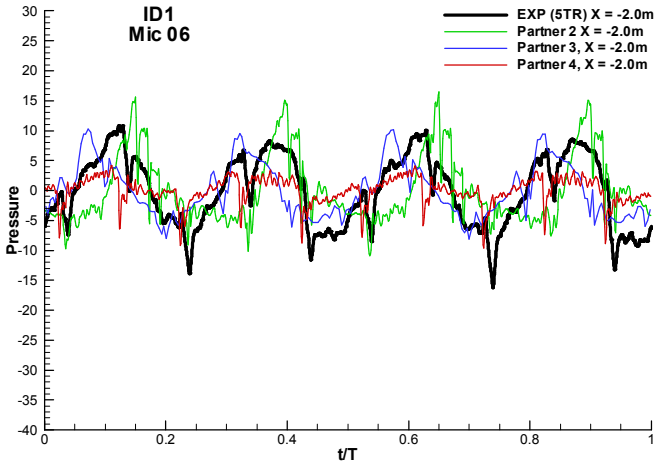

Figure 7: ID1 Acoustic pressure history ahead of main rotor

In the region where we expect tail rotor effects to be more pronounced, below the rotor on the retreating side of the main rotor, shown in Figure 8, the levels predicted by the partners are all similar as we would expect in an area dominated by the tail rotor thickness noise. There is a phase variation between the predicted results with Partner 3 showing a small variation from Partner 4 and Partner 2. The variation between the tail rotor peak levels is more likely to be due to the direct main rotor influence at this point than an interaction between main and tail rotor in this climb condition.

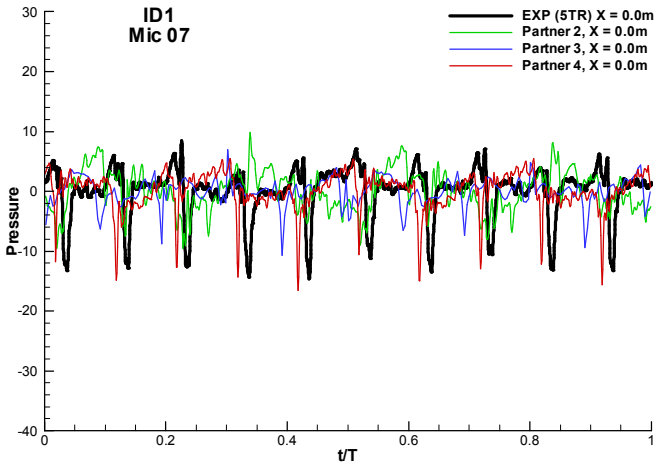

Figure 8: ID1 Pressure history below main rotor, retreating side

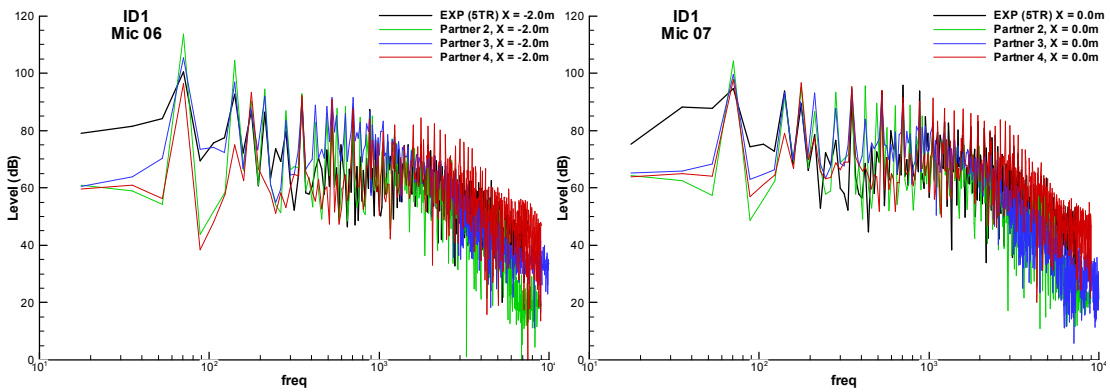

Figure 9: ID1 Spectra on advancing ahead (left) and below main rotor (right)

Figure 9 shows the spectrum for the two positions discussed above. The log scale shows most clearly the lower frequency range where all predictions show the stronger influence of the main rotor. The general agreement between partners in this frequency range is good. No partners were able to capture the higher frequency part of the spectrum which is probably generated by an impulsive self-induced BVI on the tail rotor as presented in reference [6] which discusses the aerodynamics validation.

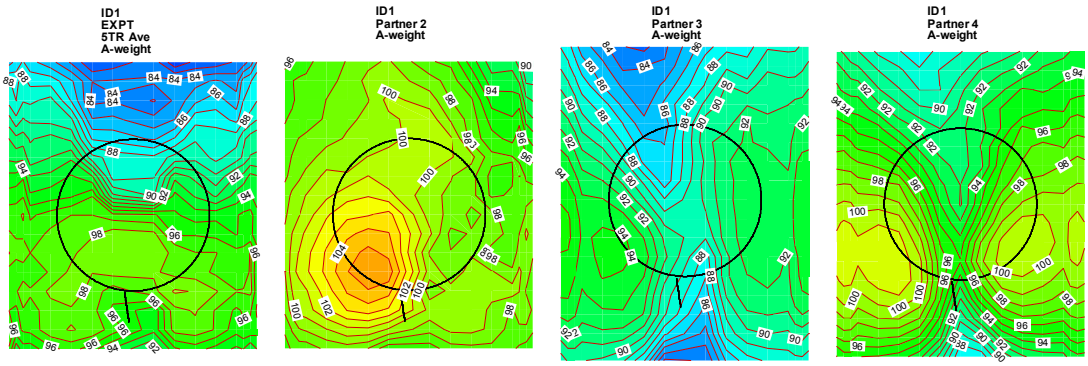

Figure 10: ID1 Noise contours

A-weighted noise contours are shown in Figure 10. There is a general agreement in the basic shape of the contours but significant differences in level. All the contour plots show the highest maximum levels on the thrust side of the tail rotor with local maxima either side of the tail rotor. The Partner 2 results show the highest levels. The low levels ahead of the helicopter in the experimental data are probably due to a fuselage/sting shielding effect not modelled in the predictions.

Case ID2; Level flight

This medium/high speed level flight test case was analysed by five partners: Partners 2-6. The following control angles and force coefficients were obtained through the application of the computational tools.

	CT_{MR}	CQ_{MR}	CT_{TR}	CQ_{TR}
EXP	0.00521	0.000328	0.00419	0.000498
Partner 2	0.00521	0.000387	0.00477	0.000256
Partner 3	0.00521	-	0.00481	-
Partner 4	0.00492	-	0.00407	-
Partner 5	0.00490	0.000310	0.00345	0.000170
Partner 6	0.00508	0.000340	0.00415	0.000240

Table 11: ID2 – Main forces and control parameters

Partners 2-4 performed computations in incompressible mode. Partner 5 used a full potential code and Partner 6's computations were corrected for compressibility by using the Prandtl-Glauert formula.

As for the climb case, the collective of the main rotor is predicted well, although in this case the tail rotor collective is under predicted, often significantly. Main rotor thrust is generally predicted well though Partner 4 and Partner 5 under predicted by similar amounts. The values for the cyclic pitch were found to vary more significantly with a range of over 5°.

As ID2 is a level flight case some interaction between main and tail rotors might be expected. Five sets of experimental results are available from a range of codes. Only the main rotor averages of the experimental data are available due to a failure of the recording of the tail rotor trigger signal for this case.

The amplitude of the pressure variations are generally larger than for the climb case with generally good agreement between the Partner 3, Partner 4 and Partner 5 results and the experimental data ahead of the main rotor on the advancing side. A strong influence is seen from the tail rotor for many of the results downstream of the main rotor. Figure 11 shows a sample time history for a region dominated by the main rotor. The results from Partner 3, Partner 4 and Partner 5 perform well, capturing the level of the pressure variation. All the codes appear to be capturing some effect of the tail rotor but with varying phase and little consistency between partner predictions. The necessity of using the main rotor average data leads to the possibility that the averaging process may have lost some of the tail rotor influences. The similar case ID13.2 discussed shortly is not subject to this failing as the 5TR averages are available.

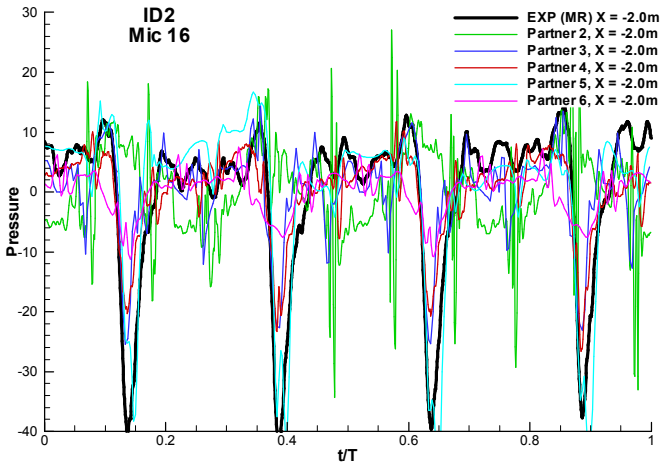

Figure 11: ID2 Pressure history ahead of main rotor on advancing side

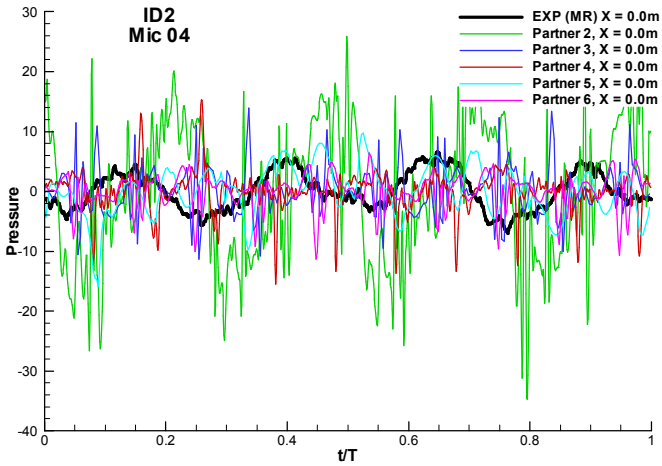

Figure 12: ID2 Pressure history below main rotor on retreating side

Looking at data for a position in the region below the tail rotor shown in Figure 12, the lack of conformity of the predictions to the experimental main rotor average can be seen. As only the main rotor average is considered here the tail rotor influence is lost within the averaging

process. There is some consistency in the level of the pressure variation within this region but no clear relationship between the predictions.

In the frequency domain, shown in Figure 13, there are some trends that can be seen for a position ahead of the main rotor on the advancing side (mic16) and in the region below the tail rotor level with the main rotor hub (mic4). The Partner 3 and Partner 6 results tend to be lower than other partners on the retreating side whilst levels are closer to the experimental results on the advancing side. Partner 3 and Partner 5 also show some lower frequency content indicating that the main rotor includes more 1/rev behaviour than predicted by other partners, with contributions at multiples of the MR rotational frequency rather than the blade passing frequency.

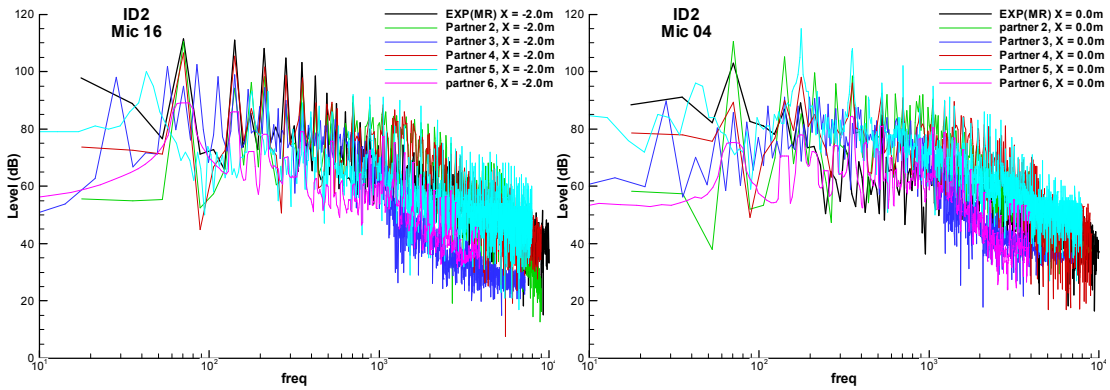

Figure 13: ID2 Spectra on advancing side ahead (left) and below main rotor (right)

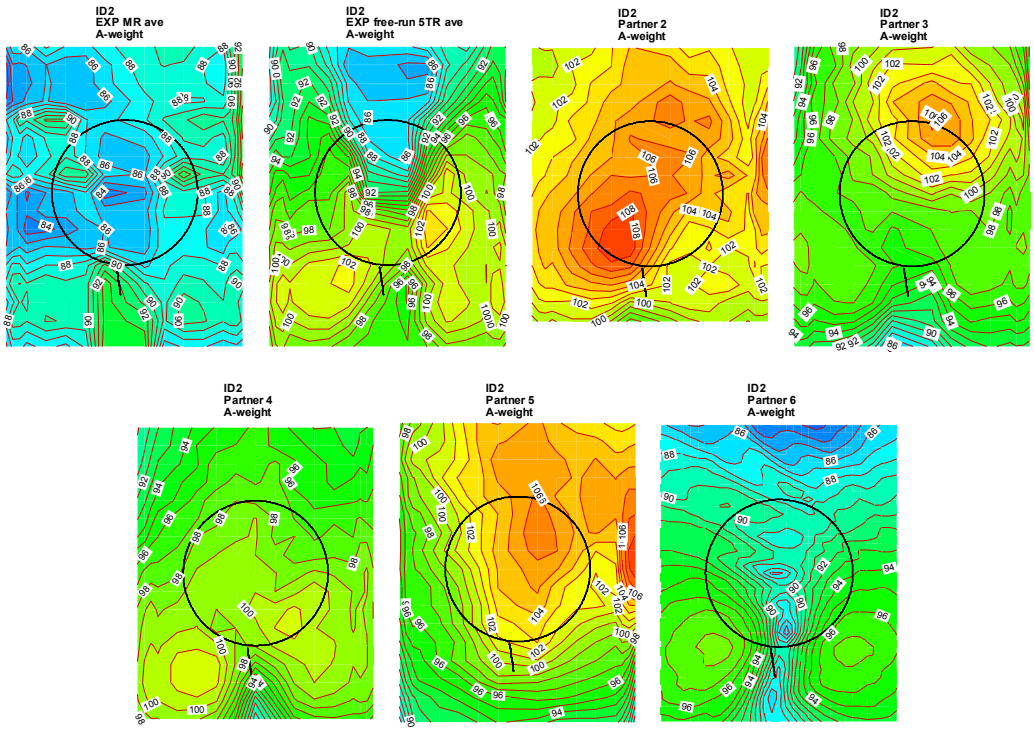

Figure 14: ID2 Noise contours

The noise level contour plots in Figure 14 show very low noise levels in the MR averaged experimental results. This is due to the A-weighting of the main rotor averaged data. For this test condition the higher frequency background and tunnel noise dominate the plot over the

lower levels of the experimental data. This is resolved by using free run data, based on a 5TR average estimated from measurements rather than from a TR triggered signal, which shows better resolution of the noise field. The 5TR average free run data are aligned well to the Partner 4 data showing two maxima, one either side of the tail rotor, with the maximum level within 2dB of the experimental data. There is also significant variation between the partners' results. Partner 2 and Partner 5 show high levels on the advancing side of the main rotor. Partner 4 and Partner 6 show local maxima each side of the tail rotor due to the tail rotor force noise. Partner 2 shows a single maximum below the tail rotor at a higher level than seen for other partners' tail rotor effects. Partner 5 shows high levels due to the main rotor which tend to obscure the tail rotor effects. This is possibly a consequence of the different dynamics resulting from different partners' trim processes.

Case ID13.2; Level flight

This test case represents a variation of the baseline test case ID2. A NACA0012 aerofoil section was employed for the tail rotor instead of the S102 aerofoil. Since the flight conditions are the same as ID2, the differences were mainly noticed for the TR aerodynamics. The test case was analysed by four partners, Partner 1, Partner 4, Partner 5 and Partner 6, and the following main control angles and force coefficients were obtained.

	CT_{MR}	CQ_{MR}	CT_{TR}	CQ_{TR}
EXP	0.00528	0.000330	0.00410	0.000541
Partner 1	0.00402	0.000321	0.00411	0.000346
Partner 4	0.00488	-	0.00380	-
Partner 5	0.0049	0.000300	0.00356	0.000160
Partner 6	0.00527	0.000358	0.00413	0.000090

Table 12: ID13.2 – Main forces and control parameters

The Partner 4 computations assumed incompressibility. Partner 1 and Partner 6's computations were corrected for compressibility by using the Prandtl-Glauert formula. Partner 5 used a full potential code. All the partners employed a force trim except for Partner 1 who applied a force trim procedure for the tail rotor and a control angle trim for the main rotor.

As expected the forces and control parameters follow similar trends to those seen for ID2. The results from Partner 1, who performed ID13.2 but not ID2, are similar to those of the other partners.

5TR averaged experimental data, triggered by the tail rotor signal, are used for this comparison. It is apparent from a comparison of Figure 11 and Figure 15, for a position ahead of the main rotor on the advancing side, that the strong peak due to the main rotor is not seen in this 5TR averaged data. This is due to a slight phase slip between the main and tail rotor rotations leading to the average filtering out the main rotor influence. Inspection of the time histories shows similar characteristics to those seen for the ID2 experimental data. Partner 1, Partner 5 and Partner 4 results capture a strong main rotor influence. This is seen clearly in behaviour in Figure 15 with Partner 5 showing the negative peaks most strongly. The Partner 6 result is aligned well to the 5TR averaged data showing only slight 4/rev behaviour without the strong main rotor peak. It is possible that a processing error has lost the main rotor effect in this acoustic calculation which is similar to this partner's results for ID2.

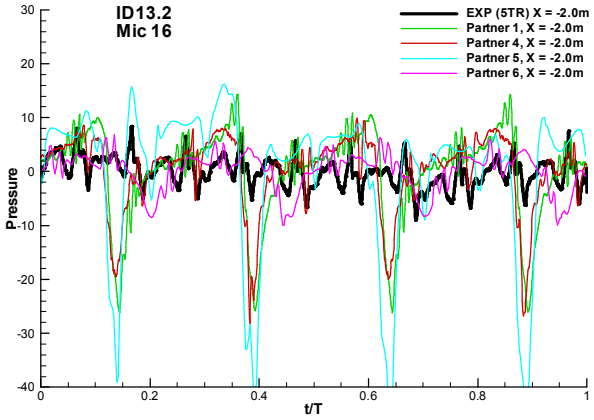

Figure 15: Pressure history ahead of main rotor on advancing side.

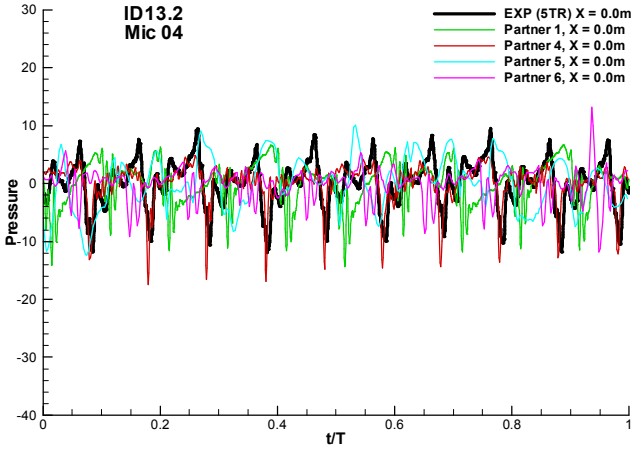

Figure 16: Pressure history below main rotor on retreating side.

In the region in which the tail rotor dominated the time history, shown in Figure 16, all the results show some good agreement with the experimental data though there is some variation in phase between the results. The results of Partner 4 capture the phase well whilst all other partners show some phase variation. All partners also show a significant departure from the 10/rev behaviour of the tail rotor showing that an influence of the main rotor flow on the tail rotor is being captured.

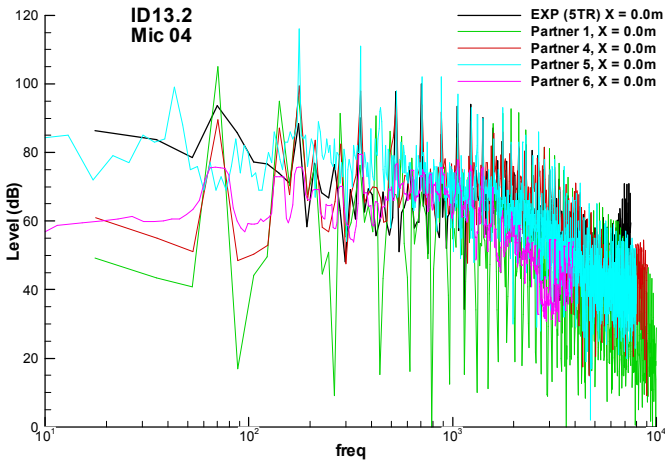

Figure 17: Spectrum below main rotor on advancing side

The spectrum, shown in Figure 17, shows the generally good agreement between all of the predictions and with the experimental data. The Partner 1 results show the best agreement across the frequency range. All the results follow the trends of the 5TR averaged experimental data although the Partner 1 and Partner 5 results show higher levels than the experimental data. This is possibly due to the high level of main rotor loading noise. Partner 5 results also show some frequency content at the blade rotational frequency due to small differences in the aerodynamic behaviour of the individual blades.

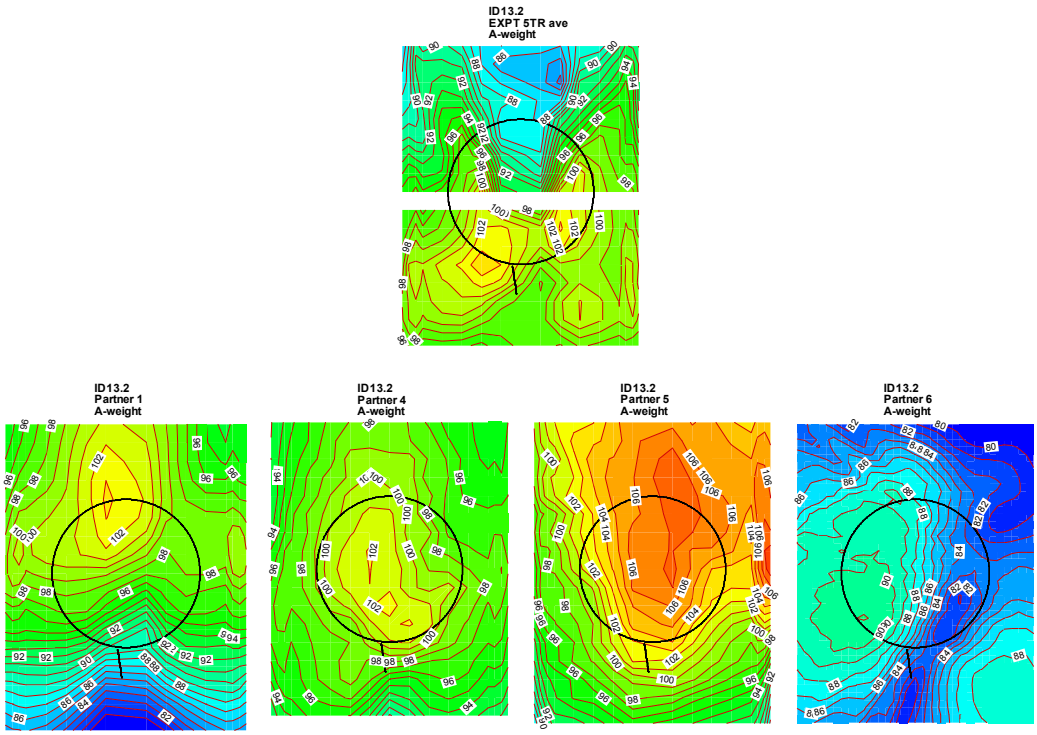

Figure 18: ID13.2 Noise contours

The noise contours in Figure 18 show a variation in behaviour. The experimental data shows the shadow directly ahead of the model as has been seen in previous figures. The gap in the experimental contour plot is due to the experimental data being captured over two runs. A maximum either side of the tail rotor is also seen. There is a sign of this behaviour in the Partner 6 data although the levels are lower than in the experimental data. The results from both Partner 1 and Partner 5 show a maximum ahead of the main rotor with Partner 5 values significantly higher than those predicted by Partner 1. Partner 4 show levels similar to those predicted by Partner 1 but the maximum is positioned less far forward.

Case ID5; Descent

ID5 is a 33m/s descent flight and is the case in which main rotor blade Vortex Interaction (BVI) is expected. This test case was analysed by Partner 1, Partner 4 and Partner 6 with Partner 1 providing solutions using both force and control angle trim methods; in this paper only the force trim results are considered. The control angles and force coefficients given in Table 13 have been obtained.

	CT_{MR}	CQ_{MR}	CT_{TR}	CQ_{TR}
EXP	0.00511	0.000142	0.00159	0.000306
Partner 1	0.00511	0.000158	0.00157	0.000248
Partner 4	0.00498	-	-	-
Partner 6	0.00499	0.000140	0.00180	0.000187

Table 13: ID5 – Main forces and control parameters

Three sets of predicted results are shown in Figure 19 with a position upstream of the main rotor on the advancing side shown on the left and a position below the tail rotor downstream of the main rotor shown on the right. The main rotor averaged experimental data is used for this case as it is expected that the main rotor noise will dominate the radiated sound field. It is clear from the extensive HeliNOVI results that very sharp fluctuations, due to MR BVI, are predicted at all but the most upstream microphone positions. At no time does the experimental averaged data produce fluctuations as large as the predictions. This may be due to some loss of peak level in the averaging process used for the experimental data. The detail for two microphone positions below the main rotor shows very strong 4/rev effects indicating that the main rotor is dominating the acoustic field, even in areas where the tail rotor influence is at its strongest.

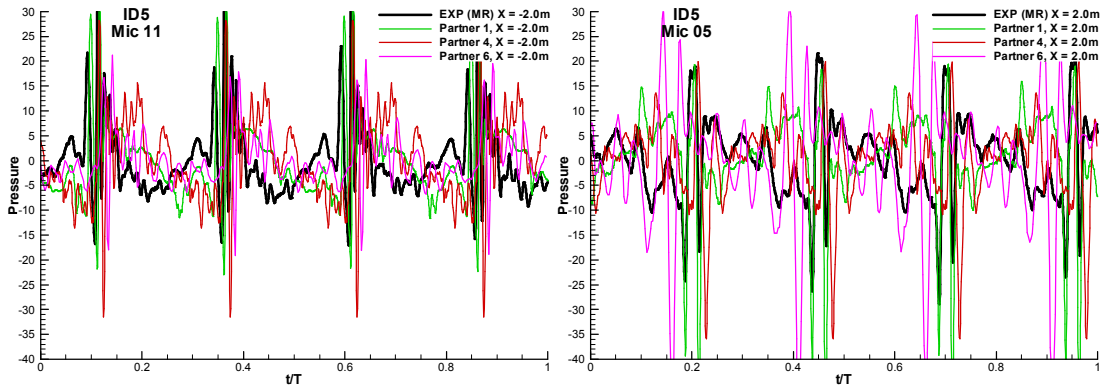

Figure 19: ID5 Pressure history advancing side/ahead and retreating side/behind main rotor

At both the positions for which results are shown in Figure 19 the main rotor BVI event is captured. There is some variation in the resulting predicted acoustics which will require detailed examination of un-averaged experimental data to resolve fully.

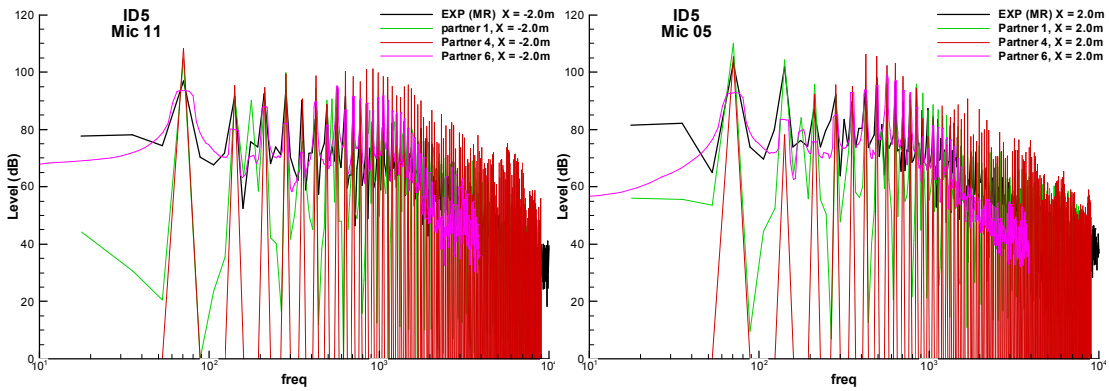

Figure 20: ID5 Pressure spectrum side/ahead and retreating side/behind main rotor

The spectrum shown in Figure 20 for the two positions already discussed shows good capture of the low frequency tones by all partners. At higher frequencies, Partner 4 tends to over predict the level compared with the averaged experimental data while Partner 6's predictions are closest to the experimental results.

Figure 21 shows the A-weighted noise contours for the ID5 case. All partners captured the general features seen in the experimental results. A strong noise contribution is present below the main rotor on the forward advancing quarter which is captured by all partners. The results from Partner 6 slightly over predict this level. The Partner 4 results produced the best agreement in level with the experimental results for this advancing side maximum. The second, slightly lower, maximum seen on the downstream retreating side of the main rotor is also best captured by Partner 4. Partner 6, with a simulation of the MR only, produced very high levels in this region indicating that this is a main rotor effect. Both Partner 1 and Partner 4 captured the peak with the Partner 1 results showing a slight over prediction.

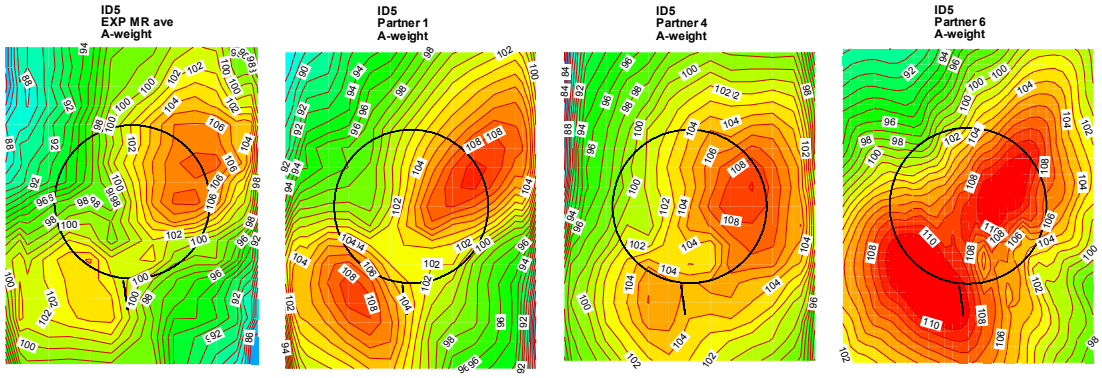

Figure 21: ID5 Noise contours

7 CONCLUSIONS

Significant effort has been expended on post test predictions, yielding a vast amount of numerical data for validation against data from the HeliNOVI test campaign. Calculations have been provided by 6 partners to cover a wide range of validation conditions. This paper has reported a first validation of all partner methodologies. The volume of high quality data, both predicted and experimental, provides the opportunity and need for additional work beyond the end of the current HeliNOVI project.

There is significant variation between partner predictions. Given the strong contribution of force noise to the total noise this is not unexpected as the different trim processes applied have given rise to significant variation in the predicted aerodynamics, as reported in [11].

The predictions generally capture the main rotor effects well as seen in the results for the descent case ID5. The strong pressure peak ahead of the main rotor on the advancing side is generally well predicted as is a secondary maximum on the downstream retreating side of the main rotor.

There is also a strong influence of force noise below the main rotor in all conditions which is highly dependent on the trim process applied. Main rotor thickness noise is seen in several results to the extreme advancing side of the microphone rake where the microphones are higher than the main rake. The tail rotor thickness noise is clearly seen below the tail rotor

position with sharp 10/rev peaks seen in most simulations. These are of similar size to those seen in the experimental data. The tail rotor force noise is also captured but shows significant variation between partners. The importance of the azimuthal increment used for the tail rotor simulations has been highlighted [11] within the HeliNOVI project and it is clear that this necessary refinement is not present in all simulations.

The lack of clear phase relationships between the main and tail rotors hinders comparison between prediction and experimental data. To account for the variation in phase between microphone measurements separate aerodynamic calculations would have to be performed for each microphone position which would make the generation of noise contours prohibitive. In the work to date, a pragmatic view has been taken that the general nature of the interaction between the rotors is independent of the phase relationship.

It is clear that there is some loss of data in the averaging process so that peak levels may not be represented accurately in the averaged data. The fact that the 5TR average does not always capture the main rotor behaviour indicates that, despite much care in the processing of the data, there is not always a good match of phase and speed between the main and tail rotors. Experimental data obtained using a model that included a fixed gearing would overcome this limitation.

The main conclusions from the work to date are:

- a valuable database of dynamic, aerodynamic and acoustic data has been generated within the HeliNOVI project for validation of acoustic prediction;
- a validation activity for acoustic prediction codes from 6 partners (CIRA, DLR, EC, ECD, NTUA and QinetiQ) has been performed;
- force noise often dominates the results so that the trim methodology is crucial to the prediction;
- all codes have captured the influence of the tail rotor in their simulations and an influence of the main rotor on the tail rotor;
- the results from each code reveal that the influence of main and tail rotors is being captured within the predicted results, but no one code captures the full directivity of the acoustics for all validation cases;
- some issues remain regarding the averaged experimental data and phase relationships;
- a further validation opportunity exists for individual partners beyond the current project and is recommended. Validation against un-averaged data would clarify the phase relationship and provide peak levels.

8 ACKNOWLEDGEMENTS

The HeliNOVI project is generously supported by the European Union under the Competitive and Sustainable Growth Programme in the 5th Framework, Contract Nr. G4RD-CT-2001-40113. Special thanks go to the engineers, technicians, and mechanics of DLR, DNW and NLR for their tireless efforts in preparation and conduction of this highly complex test.

9 REFERENCES

[1] DLR, "*HeliNOVI – Annex I: Description of Work*", September 2001.

[2] Voutsinas, S., Visingardi, A., Yin, J., Arnaud, G., Falchero, Dummel, A., Pidd, and M., Prospathopoulos, J., "*Aerodynamic Interference in Full Helicopter Configurations and Assessment of Noise Emission: Pre-test Modeling Activities for the HeliNOVI*

Experimental Campaign", 31st European Rotorcraft Forum 2005, 13th-15th September 2005, Florence, Italy.

[3] Schneider, O., "*Test Data Analysis of WP2 SPR Measurements*", HeliNOVI deliverable D2.3 -2.5, October 2005.

[4] Langer, H.-J., Dieterich, O., Oerlemans, S., Schneider, O., Van der Wall, B. and Yin, J., "*The EU HeliNOVI Project - Wind Tunnel Investigations for Noise and Vibration Reduction*", 31st European Rotorcraft Forum, Florence, Italy, September 13-15, 2005.

[5] Yin, J., Van der Wall, B., Oerlemans, S., et al: "*Representative Test results from HELINOVI Aeroacoustic Main Rotor/Tail Rotor/Fuselage Test in DNW*", 31st European Rotorcraft Forum, Florence, Italy, September 2005.

[6] Visingardi, A., Dummel, A., Falchero, D., Pidd, M., Voutsinas, S.G., Yin, J., "*Aerodynamic interference in full helicopter configurations: validation using the HeliNOVI database*"; 32nd European Rotorcraft Forum; 12 – 14 September 2006, Maastricht, The Netherlands.

[7] Yin, J., Dummel, A., Falchero, D., Pidd, M., Prospathopoulos, J., Visingardi and A., Voutsinas, S.G. "*Analysis of Tail Rotor noise reduction benefits using HELINOVI aeroacoustic main/tail rotor test and posttest prediction results*", European Rotorcraft Forum; 12 – 14 September 2006, Maastricht, The Netherlands.

[8] Dieterich, O., "*Wind Tunnel Model Database*", HeliNOVI deliverable D2.1-1, September 2002.

[9] Stephan, M., Klöppel, V. and Langer, H.J., "*A new wind tunnel test rig for helicopter testing*", 14th European Rotorcraft Forum, 1988.

[10] Pidd, M, "*Final Validation Report of the Acoustic Prediction Codes*", HeliNOVI deliverable D1.4-3, December 2005.

[11] Visingardi, A, "*Final Validation Report of the Aerodynamic Prediction Codes*", HeliNOVI deliverable D1.4-2, January 2006.

[12] Brentner, K.S. and Farassat, F., "*Modeling aerodynamically generated sound of helicopter rotors*", Progress in Aerospace Sciences 39 (2003) 83-120.